

# Synchronization patterns in LIF Neuron Networks: Merging Nonlocal and Diagonal Connectivity

N. D. Tsigkri-DeSmedt

*Institute of Nanoscience and Nanotechnology, National Center for Scientific Research “Demokritos”, GR-15341 Athens, Greece and  
Section of Solid State Physics, Department of Physics,  
National and Kapodistrian University of Athens, GR-15784 Athens, Greece*

I. Koulterakis and G. Karakos

*Institute of Nanoscience and Nanotechnology, National Center for Scientific Research “Demokritos”, GR-15341 Athens, Greece and  
School of Electrical Engineering and Computer Science,  
National Technical University of Athens, GR-15780 Athens, Greece*

A. Provata

*Institute of Nanoscience and Nanotechnology, National Center for Scientific Research “Demokritos”, GR-15341 Athens, Greece  
(Dated: Received: date / Revised version: date)*

**Abstract:** The effects of nonlocal and reflecting connectivities have been previously investigated in coupled Leaky Integrate-and-Fire (LIF) elements, which assimilate the exchange of electrical signals between neurons. In this work we investigate the effect of diagonal coupling inspired by findings in brain neuron connectivity. Multi-chimera states are reported both for the simple diagonal and combined nonlocal-diagonal connectivities and we determine the range of optimal parameter regions where chimera states appear. Overall, the measures of coherence indicate that as the coupling range increases (below all-to-all coupling) the emergence of chimera states is favored and the mean phase velocity deviations between coherent and incoherent regions become more prominent. A number of novel synchronization phenomena are induced as a result of the combined connectivity. We record that for coupling strengths  $\sigma < 1$  the synchronous regions have mean phase velocities lower than the asynchronous, while the opposite holds for  $\sigma > 1$ . In the intermediate regime,  $\sigma \sim 1$ , the oscillators have common mean phase velocity (i.e., are frequency-locked) but different phases (i.e., they are phase-asynchronous). Solitary states are recorded for small values of the coupling strength, which grow into chimera states as the coupling strength increases. We determine parameter values where the combined effects of nonlocal and diagonal coupling generate chimera states with two different levels of synchronous domains mediated by asynchronous regions.

## I. INTRODUCTION

The neuron network of the brain is characterized by complex architecture at many scales of hierarchy, which are still not fully recorded. The complexity of the connectivity gives rise to intricate synchronization phenomena between different parts of the brain, which drive the exchange of information and which are at the basis of common brain functions (cognition, memory etc.) [1–3]. To unravel the influence of the neuron network connectivity in brain functionality, large scale simulations of neuron networks are undertaken by international collaborations, which model the exchanges of electrical and chemical signals in the brain [4, 5]. The ultimate goal is to establish the missing link between brain structure (anatomy, neuron network connectivity, synchronization patterns) and functionality (perception, cognition, memory) [6–12]. In this direction specific models describing single neuron activity are employed, accompanied with connectivity rules inspired by biological neuron networks. Single neurons, characterized by spiking or bursting activity, are modeled by a number of nonlinear schemes, such as the Hodgkin-Huxley model, the Hindmarsh-Rose

model, the FitzHugh-Nagumo model and the various LIF schemes [13–15]. Commonly used linking schemes employed in the literature belong to two categories: deterministic or stochastic. Deterministic connectivity in neuron networks ranges from the most local nearest-neighbor coupling, to distant nonlocal coupling, global coupling, field coupling schemes and even multilayer (multiplex) networks [15–22]. In parallel, stochastic connectivity schemes have been studied, such as Erdős-Rényi networks, small world connectivity and scale free linking [19, 23, 24]. The biologically inspired models, equipped with the appropriate connectivity schemes, aim to detect the different levels of spatiotemporal organization and to identify synchronization patterns which are characteristic of the functional modes of the brain.

A recently discovered [25, 26] complex synchronization pattern is the chimera state; this is a collective state characterized by the simultaneous presence of synchronous and asynchronous domains [18, 19, 27–32]. Chimera states have been realized using a number of neuron models, such as the FitzHugh-Nagumo model [19, 24, 32–35], the Hindmarsh-Rose model of bursting neurons [20–22, 29, 36–39], the LIF model [34, 40–44] and others. More recent studies include simulations of chimera ra

states in 2D lattices [34, 38] and 3D spatial dimensions [34, 39, 44–46]. Another striking synchronization example is the subthreshold oscillations: the network splits into two coexisting domains, one domain where all elements perform small-amplitude oscillations at subthreshold values and one domain where the incoherent elements develop a multileveled mean phase velocity distribution [43].

In previous studies of the Leaky Integrate-and-Fire (LIF) dynamics, a plethora of intriguing synchronization phenomena have been reported for coupled LIF networks with nonlocal coupling [40–43, 47]. A few examples are briefly discussed below.

- The case of negative (repulsive) coupling constant was studied using a nonlocal kernel. This connectivity produced multichimera states whose multiplicity (number of coherent/incoherent domains) depends on the coupling strength [42, 43, 47].
- In the case of positive (attracting) nonlocal diffusive coupling, travelling waves of synchronous elements with constant phase difference were produced, while chimera states were difficult to identify. Subthreshold oscillations were observed, where the number of oscillators staying below the threshold is statistically constant in time and only depends on the coupling strength [43]. Their potential values fluctuate erratically around a central point located below the fixed point of the uncoupled neuronal oscillator. Note that in biological neuron networks subthreshold oscillations have been experimentally recorded as rhythmic fluctuations of the voltage difference between the interior and exterior of a neuron [6, 7].
- Hierarchical topology in the coupling was investigated and it was shown to induce nested chimera states and transitions between multichimera states with different multiplicities [47]. The use of hierarchical connectivity was motivated by previous analyses of MRI and fMRI images of the brain which reveal that the neuron axons are distributed fractally in the brain [10–12].
- In ref. [43] the case of reflecting connectivity was studied, where each neuron is coupled with a number of other neurons located perpendicularly opposite, through a specific axis of the ring. For this connectivity, novel incoherent domains coexisting with subthreshold elements were found. For large values of the coupling strength the full oscillations are restricted in one half of the ring, while the elements of the other half perform small-amplitude, subthreshold oscillations [43]. The use of the reflecting connectivity was inspired by the work of [1], where the recorded neuron connectivity patterns are used as fingerprints for identifying individuals.

The results in ref. [1] which motivated the use of the reflecting connectivity in ref. [43] are also on the basis of the present study. The brain neuron network analysis in [1] addresses the connectivity profiles for the identification of an individual, on the basis of eight functional networks. In order to quantify edgewise contributions for the identification of an individual the authors suggested a measure termed Differential Power (DP). The DP value quantifies how “characteristic” a particular edge tends to be. DP connections that characterize a) individuals across conditions or b) across individuals regardless of condition, appear between regions in one hemisphere and regions in the other hemisphere, arranged diagonally opposite to each other. These diagonal edges (connections) are characteristic of each individual and are good candidates for identifying individuals (fingerprints). In the opposite case, the measure Group Consistency (denoted by  $\Phi$ ) was introduced which quantifies the consistency of a connection within a subject and across a group.  $\Phi$  connections that are consistent across a group, appear to link the two hemispheres perpendicularly to the plane separating them. They are common to all individuals, they constitute the major parts of connections and consequently cannot be used to identify individuals.

Following the study on the reflecting connectivity which gave rise to subthreshold oscillations [43] and which was inspired by the  $\Phi$  connections of Ref. [1], we now turn to diagonal and nonlocal coupling schemes, inspired by the DP connections in the same reference. Each neuron will be now connected with  $2R_{diag}$  neurons symmetrically distributed across a standard mirror diameter of the ring (symmetry about the center). We also consider combined nonlocal-diagonal linking where each element is linked with a number of neurons  $R_{nl}$  on its left and  $R_{nl}$  on its right in addition to the diagonal ones. This is inspired by the fact that neurons can be simultaneously interconnected in their structural areas and functionally linked with other regions of the brain as indicated in [48]. The novelty of the present study lies not only in the use of the particular, biologically-inspired connectivities, but also on the novel synchronization phenomena induced. Namely, a) the appearance of solitary states which gradually give rise to chimera states as the coupling strength increases, b) the interesting bi-leveled chimeras where two levels of synchronization appear and the incoherent regions are located between them and c) the inversion of coherence for large values of the coupling strength  $\sigma$ : for small (large) values of  $\sigma$  the frequency of the coherent regions is lower (higher) than the incoherent ones.

This work is organized as follows: In section II we recapitulate the main properties of the single LIF model and we introduce the nonlocal and diagonal coupling. In section III we explore the network synchronization motifs when simple diagonal connectivity is assigned. In section IV A and B we scan the parameter space and discuss the effects of the combined connectivity scheme on the dynamical behavior of the system. In section IV C we

scan the parameter region where bi-leveled synchronous domains appear and we discuss the mechanisms responsible for this effect. In the concluding section we propose future steps of this study and we summarize our main results.

## II. LEAKY INTEGRATE-AND-FIRE MODEL WITH LINEAR COUPLING

To study the dynamical evolution and the synchronization phenomena in a system of  $N$  neurons we use the Leaky Integrate-and-Fire (LIF) model [49, 50], which describes the dynamics of single neurons. The LIF model exhibits an exponential increase of the potential followed by an abrupt resetting to the rest state. The evolution of the membrane potential  $u(t)$  of a single neuron is represented by the following equations:

$$\frac{du(t)}{dt} = \mu - u(t) \quad (1a)$$

$$\lim_{\epsilon \rightarrow 0^+} u(t + \epsilon) \rightarrow u_0, \quad \text{when } u(t) \geq u_{\text{th}} \quad (1b)$$

where  $\mu$  defines the spiking rate and  $u_{\text{th}}$  denotes the threshold value of the potential, which when exceeded,  $u$  is restored to its ground state  $u_0$ . Assuming, without loss of generality, that at time  $t = 0$  the potential is at  $u_0$  and that the resetting to the ground state is abrupt, the period  $T_s$  of the single neuron is calculated from Eq. 1 as  $T_s = \ln[(\mu - u_0)/(\mu - u_{\text{th}})]$ .

For the network of interacting neurons we use linear coupling between neurons  $j$  and  $i$  and the coupling is defined by the adjacency or coupling matrix  $\sigma(i, j)$ . For a number of  $N$  LIF elements, each of them having potential  $u_i(t)$ ,  $i = 1, \dots, N$  and connected on a ring topology the network dynamics is described by the following equations:

$$\frac{du_i(t)}{dt} = \mu - u_i(t) - \frac{1}{N_i} \sum_{j=1}^{N_i} \sigma(i, j) [u_j(t) - u_i(t)] \quad (2a)$$

$$\lim_{\epsilon \rightarrow 0^+} u_i(t + \epsilon) \rightarrow u_0, \quad \text{when } u_i(t) \geq u_{\text{th}}, \quad (2b)$$

where  $N_i \leq N$  is the total number of elements that are linked to element  $i$ . The parameters  $N_i$  may be different for each element but in this study we assume that  $N_i = N_c$  is kept constant for all elements. Moreover, in Eq. (2) we assume that all elements have as common parameters (properties) the threshold potential  $u_{\text{th}}$ , the spiking rate  $\mu$ , the rest potential  $u_0 = 0$ , while they start from different (usually random) initial conditions (potentials). Regarding the connectivity matrix  $\sigma(i, j)$  we consider here the following two cases: simple diagonal

connectivity and combined nonlocal-diagonal connectivity. In the first case the matrix element  $\sigma_d(i, j)$  linking node  $j$  to  $i$  takes the form:

$$\sigma_d(i, j) = \begin{cases} \sigma & \text{for } (\frac{N}{2} + i - R_{\text{diag}}) \leq j \leq (\frac{N}{2} + i + R_{\text{diag}}) \\ 0 & \text{otherwise} \end{cases} \quad (3)$$

where  $\sigma$  is a positive constant and all indices are understood  $\text{mod } (N)$ . In Fig. 1 every element is only linked to  $2R_{\text{diag}} + 1$  neighbors (red, dark-colored) across the diagonal of the ring. The ratio of the linked elements to the total system size is the coupling ratio which is denoted by  $d = (2R_{\text{diag}} + 1)/N$  and will be used as one of the system parameters in the sequel.

In the case of the combined (nonlocal-diagonal) connectivity the adjacency matrix  $\sigma_c(i, j)$  takes the form

$$\sigma_c(i, j) = \begin{cases} \sigma & \text{for } (\frac{N}{2} + i - R_{\text{diag}}) \leq j \leq (\frac{N}{2} + i + R_{\text{diag}}) \\ \sigma & \text{for } i - R_{\text{nl}} \leq j \leq i + R_{\text{nl}} \\ 0 & \text{otherwise.} \end{cases} \quad (4)$$

Here, similarly to Eq. 3,  $\sigma$  is positive and all indices are understood  $\text{mod } (N)$ . In this scheme every element is linked to its  $R_{\text{nl}}$  neighbors on its left, to its  $R_{\text{nl}}$  neighbors on its right and also to  $2R_{\text{diag}} + 1$  neighbors across the diagonal of the ring, i.e., all red (dark) and yellow (grey) colored elements in Fig. 1. This means that every element will be linked to a total of  $(2R_{\text{diag}} + 2R_{\text{nl}} + 1)$  nodes. To avoid introducing many parameters we hereafter consider the case where  $R_{\text{diag}} = R_{\text{nl}} = R$ , thus the number of total elements to which each element is linked, is equal to  $4R + 1$ . The coupling ratio in the case of combined connectivity is  $d = (4R + 1)/N$ .

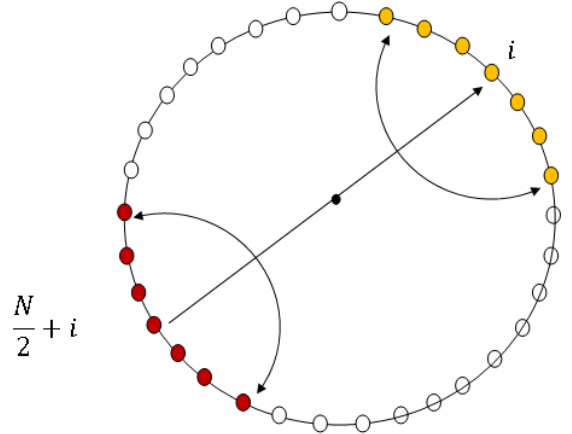


FIG. 1: (Color online) Nonlocal and diagonal connectivity scheme. In the diagonal connectivity scheme every element  $i$  is linked with  $2R_{\text{diag}} + 1$  neighbors across the diagonal of the ring (red, dark nodes), while in the combined connectivity scheme  $i$  is linked, additionally, with  $R_{\text{nl}}$  other elements to its left and  $R_{\text{nl}}$  elements to its right (yellow, grey nodes). The connectivity range here is  $R = 3$  (with  $R_{\text{diag}} = R_{\text{nl}}$ ).

Synchronization properties are quantitatively described by the mean phase velocity  $\omega_i$  of element  $i$ . If

the system is integrated for time  $\Delta T$ , we compute the number of full cycles  $k_i$  which element  $i$  has completed during time  $\Delta T$ . The mean phase velocity, or average frequency  $\omega_i$  of element  $i$  is then estimated as follows [33]:

$$\omega_i = \frac{2\pi k_i}{\Delta T} \quad (5)$$

Qualitatively, synchronization patterns and chimera states are represented by the space-time plots. Space-time plots are color coded plots that show the evolution of the oscillator potentials in time and in space. These are particularly useful for monitoring transitions between different synchronization patterns or travelling chimeras, when the mean phase velocities do not give meaningful results.

We complement our study with the calculation of the relative size of the incoherent parts  $N_{\text{incoh}}$  and with the extensive cumulative size  $M_{\text{incoh}}$  which represents the degree of incoherence of the chimera states [24]. The quantities  $N_{\text{incoh}}$  and  $M_{\text{incoh}}$  are defined as follows:

$$N_{\text{incoh}} = \frac{1}{N} \sum_{i=1}^N \Theta(A) \quad (6a)$$

$$A = \begin{cases} \omega_i - \omega_{\text{coh}} - c, & \text{when } \omega_{\text{coh}} < \omega_{\text{incoh}} \\ \omega_{\text{coh}} - \omega_i - c, & \text{when } \omega_{\text{coh}} > \omega_{\text{incoh}} \end{cases} \quad (6b)$$

$$M_{\text{incoh}} = \sum_{i=1}^N |(\omega_i - \omega_{\text{coh}})|. \quad (7)$$

In Eqs. 6 and 7,  $\omega_i$  denotes the mean phase velocity of the  $i$ -th element and  $\omega_{\text{coh}}$  the common mean phase velocity of the coherent parts.  $\Theta$  is the step function which takes the value 1 when its argument is positive and zero otherwise. To account for the fluctuations at the level of coherent parts a small tolerance is included in the calculations when computing the measures  $M_{\text{incoh}}$  and  $N_{\text{incoh}}$ . This is represented by parameter  $c$  which is set to 0.05. Note that the case of complete synchronization is obtained when  $M_{\text{incoh}} = 0$  and  $N_{\text{incoh}} = 0$ .

Previous studies have shown that different connectivity schemes result in different dynamical behavior. We present, in Fig. 2, typical results for different connectivity schemes, namely for a) nonlocal connectivity, b) reflecting connectivity c) diagonal connectivity and d) combined nonlocal and diagonal connectivity. Note that all four cases are simulated under common parameters and only the links are placed differently in the network. This figure demonstrates explicitly how influential the connectivity in synchronization is. In the next sections our focus will be on how simple diagonal and combined nonlocal-diagonal connectivities affect the dynamics of

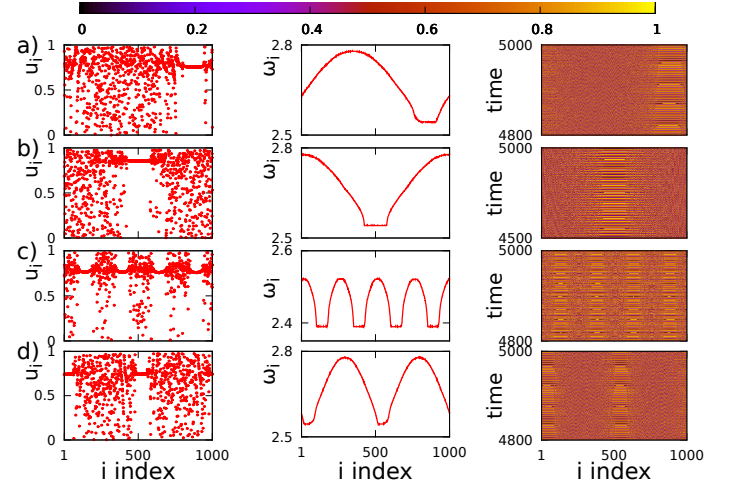


FIG. 2: (Color online) LIF system with different connectivity schemes and for the same number of connection,  $R_{\text{total}} = 600$  links ( $d = 0.6$ ): Typical snapshots (left column), mean-phase velocity (middle column) and space-time plots (right column). a) Nonlocal connectivity, b) reflecting connectivity, c) diagonal connectivity and d) combined nonlocal-diagonal connectivity. Other parameters are common:  $\sigma = 0.6$ ,  $N = 1000$ ,  $\mu = 1$  and  $u_{\text{th}} = 0.98$ . All realizations start from the same initial conditions, randomly chosen between 0 and  $u_{\text{th}}$ .

the LIF network. Throughout this work the parameter space of the coupling range and the coupling strength is scanned. Other working parameters are kept to values  $\mu = 1.0$ ,  $u_{\text{th}} = 0.98$ ,  $u_0 = 0.0$ , common for all elements. We assume that the elements always start with initial potentials randomly distributed in the interval  $[0, u_{\text{th}}]$ .

### III. EFFECTS OF DIAGONAL COUPLING

Although simple diagonal coupling is not common in natural networks where the elements tend to connect to their neighbors before linking with distant nodes, for reasons of completeness we choose to study first the case of simple diagonal connectivity before investigating the combined one. As in the case of usual, nonlocal connectivity we keep symmetry in the linking arrangement. In a ring network of size  $N$ , the elements coupled to a node  $i$  are symmetrically placed around the diagonal node  $N/2 + i$  (modulo  $N$ ), see Fig. 1 (red, dark nodes). The coupling matrix is given by Eq. 3, with  $R_{\text{diag}} = R$  common to all elements. In the next two subsections we present the synchronization phenomena which are induced as we vary the coupling strength, sec. III A and the coupling range, sec. III B.

### A. Diagonal connectivity with coupling strength variations

For diagonal connectivity, multi-chimera states are observed whose multiplicity depends on the size of the coupling strength. As an example, for fixed coupling range  $R = 300$  we plot in Fig. 3 the potential profiles (left), the mean phase velocities (middle) and the spacetime plots (right), for three different values of  $\sigma = 0.4, 1, 1.4$ . We recognize a four-headed chimera for  $\sigma = 0.4$ , an asynchronous state for  $\sigma = 1.0$  and an asymmetric chimera for  $\sigma = 1.4$ . It is remarkable that for  $\sigma < 1$  the synchronous regions have lower mean phase velocities than the asynchronous ones, while the opposite is true for  $\sigma > 1$ . In the case  $\sigma = 1$  all oscillators have the same mean phase velocity, but different phases; they are frequency-synchronous but remain phase-asynchronous. The reversion of the synchronous-asynchronous levels has been also observed by Omelchenko et al. [51] for nonlocally coupled the Van der oscillators, when the coupling constant exceeds a certain threshold. The present results show that it is a general property of the LIF model and has been previously reported in Ref. [34] for the 2D connectivity. The same effect also holds for the combined (nonlocal-diagonal) connectivity, as we will see in sec. IV.

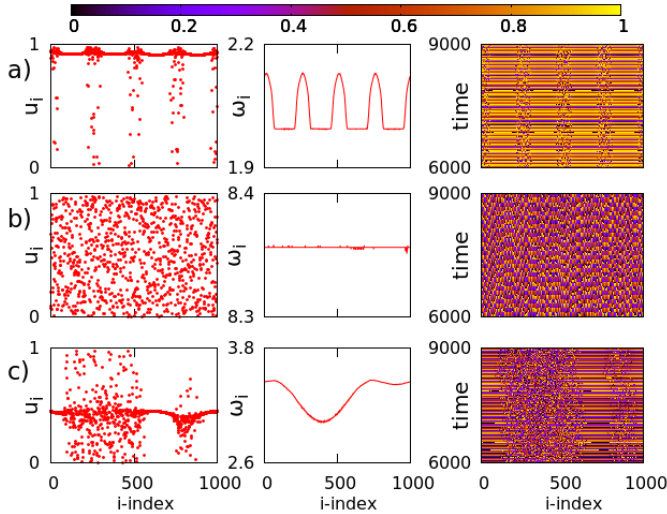


FIG. 3: (Color online) LIF system with simple diagonal connectivity: Typical snapshots (left column), mean-phase velocity (middle column) and space-time plots (right column). a)  $\sigma = 0.4$ , b)  $\sigma = 1.0$ , c)  $\sigma = 1.4$ . Other parameters are  $R=300$  ( $d=0.601$ ),  $N = 1000$ ,  $\mu = 1$  and  $u_{th} = 0.98$ . All realizations start from the same initial conditions, randomly chosen between 0 and  $u_{th}$ .

The reversion of the synchronization levels is clearly shown in Fig. 4, where all measures of coherence present transition points around  $\sigma \sim 1$ . In panel 4a the average  $\langle \omega_{coh} \rangle$  of the coherent regions increases as a function of  $\sigma$  for  $\sigma < 1$ . In the vicinity of  $\sigma \sim 1$  an extremum is observed, while for  $\sigma > 1$  the average  $\langle \omega_{coh} \rangle$  slightly decreases. Similarly, in Fig. 4c the difference  $\Delta\omega$  be-

tween coherent and incoherent regions cross the 0-axis for  $\sigma \sim 1$ . Around the same transition point the number of incoherent elements  $\langle N_{incoh} \rangle$  vanishes (see Fig. 4b) and so does the index  $\langle M_{incoh} \rangle$  which accounts for the area (in the  $\sigma - \omega$  graph) between coherent and incoherent regions (see Fig. 4d).

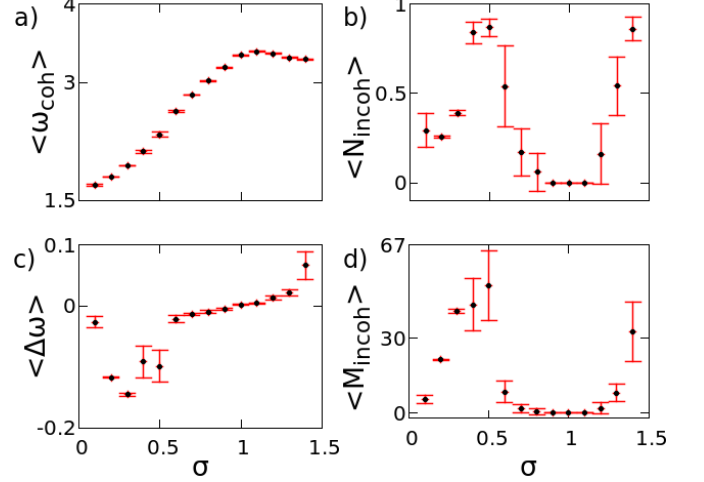


FIG. 4: (Color online) LIF system with simple diagonal connectivity: Measures of coherence and incoherence for different values of the coupling strength and for  $R = 200$ . Other parameters as in Fig. 3.

### B. Diagonal connectivity with coupling range variations

As previously shown in the literature the coupling range plays a special role in controlling the multiplicity of the chimera state [33, 47, 52]. In particular, as we increase the coupling range the number of coherent(incoherent) regions decreases. The same is true here, although the position of the coupled nodes is diagonally opposite to one another. In fact, for small values of  $R$  no chimera states are observed, see Fig. 5a. The same is true in the case of classical nonlocal connectivity, when the elements are linked only with a few nearest neighbors in their immediate vicinity [24, 33, 42, 47]. As the value of  $R$  increases the coupling causes organization in small regions and a number of coherent/incoherent regions are formed, see Fig. 5b. As the coupling range increases further, the multiplicity of the chimeras decreases as can be seen in Fig. 5c (see also Fig. 3c for comparison). The appearance of incoherent regions of different sizes is a new effect, which could be attributed due to the delocalization of the interactions (diagonal linking) and to an instability created in the middle of a coherent region giving rise to “rebels” forming gradually incoherent domains.

The measures of coherence also indicate here transitive behavior in the parameter region  $150 < R < 300$ . In particular, for small values of the coupling range  $R$ ,



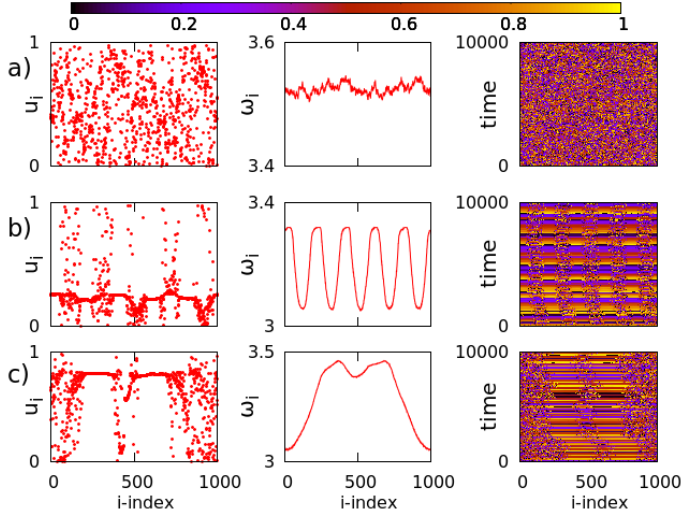


FIG. 5: (Color online) LIF system with simple diagonal connectivity: Typical snapshots (left column), mean-phase velocity (middle column) and space-time plots (right column). a)  $R = 10$  ( $d=0.041$ ), b)  $R = 250$  ( $d=0.501$ ), c)  $R = 330$  ( $d=0.661$ ). Parameters are  $\sigma = 1.4$  and others as in Fig. 3.

all elements present common  $\omega$ 's with some fluctuations as can be seen from Fig. 6c, indicating that  $\Delta\omega \simeq 0$ . Regardless of the common frequency, in this parameter range the oscillator phases remain asynchronous as can be seen in Fig. 5a (left and right panels). As the coupling range increases the average mean phase velocity decreases due to the effort of the elements to organize, see Fig. 6a. Around  $R \sim 150$  a transition region begins, where all measures increase, while after  $R \sim 300$  all measures do not show significant change with  $R$ .

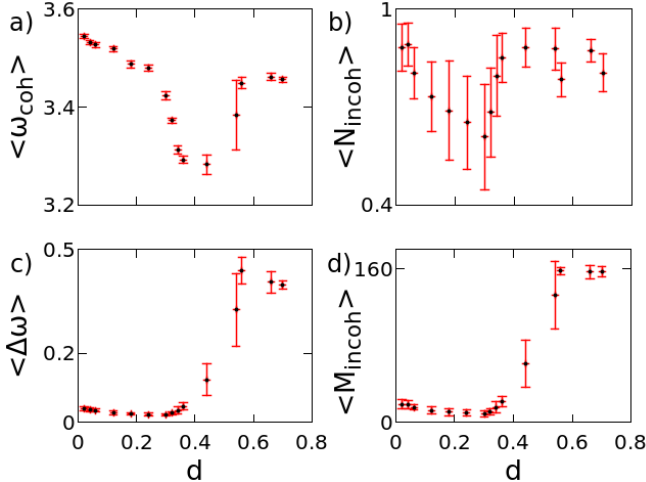


FIG. 6: (Color online) LIF system with simple diagonal connectivity: Measures of coherence-incoherence for different values of the coupling range.  $d$  is the coupling ratio,  $\sigma = 1.4$  and all other parameters are as in Fig. 3.

#### IV. EFFECTS OF COMBINED NONLOCAL AND DIAGONAL COUPLING

Turning to the case of combined nonlocal-diagonal connectivity which is more relevant in biological processes, in the next subsections we present the synchronization phenomena observed as we vary the coupling range (sec. IV A) and the coupling strength (sec. IV B). In particular, parameter changes induce solitary states and a variety of chimeras which differ mainly in their multiplicity and the size of the (in)coherent domains.

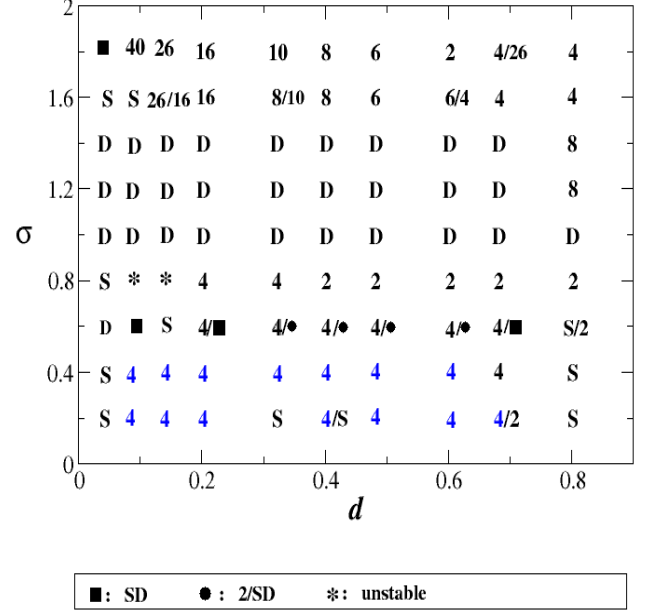


FIG. 7: Mapping of the chimera multiplicity on the  $(d - \sigma)$  parameter space. The numbers correspond to the multiplicity of the chimeras, the letters “D” and “S” denote desynchronization and synchronization respectively, and the stars mark unstable chimera states. The blue color denotes solitary states; these states are found for  $\sigma \leq 0.4$ , for most values of  $R$  and have multiplicity 4. For other notation see the legend.

In Fig. 7 we present collectively in the  $(d - \sigma)$  parameter space the quantitative results of our study, while the details of the simulations and discussion of the results are given in secs. IV A and IV B. For different pairs of  $(d, \sigma)$  on the map we indicate the multiplicity of the corresponding chimera. For example, in position  $(d = 0.2, \sigma = 0.8)$  a four-headed chimera is observed and thus the number “4” appears in the corresponding position of the map. In the cases of smaller  $\sigma$ , i. e.  $\sigma = 0.2 - 0.4$  the patterns are chimera-like; they consist of mostly synchronous elements with spurious isolated unsynchronized elements (or small asynchronous regions) also known as “solitary states” [53–55]. In Fig. 7 solitary states are denoted with blue color; they are found for  $\sigma \leq 0.4$  and their multiplicity is 4. In some cases two numbers appear in the same position of the plot;

this means that different simulations resulted in different states: see for example ( $d = 0.6$ ,  $\sigma = 1.6$ ), where the indication “6/4” appears in the corresponding position. In this case some simulations resulted in two-headed chimeras while others in four-headed ones. Note that these double values appear in the boundaries between domains where multiplicity changes. The character “S” corresponds to complete synchronization, the character “D” to complete desynchronization, while the stars, \*, denote unstable chimeras (meaning chimera are formed but do not settle) for these simulation times. All results in Fig. 7 are based on 14 independent simulations for each pair ( $d, \sigma$ ). More detailed description and quantitative features of the patterns follow in the next two subsections.

### A. Combined Connectivity with variation of the coupling range

In this subsection we discuss the results on the morphology of chimera states and other synchronization patterns by systematically changing the coupling range  $R$ .

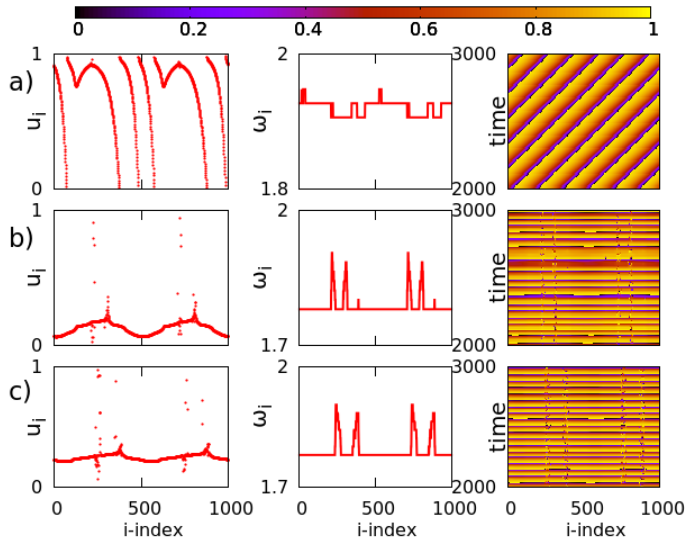


FIG. 8: (Color online) LIF system with superposition of nonlocal and diagonal connectivity: Typical snapshots (left column), mean-phase velocity (middle column) and space-time plots (right column). a)  $R = 10$  ( $d = 0.041$ ), b)  $R = 100$  ( $d = 0.401$ ) and c)  $R = 170$  ( $d = 0.681$ ). Other parameters are  $\sigma = 0.4$ ,  $N = 1000$ ,  $\mu = 1$ , and  $u_{th} = 0.98$ . All realizations start from the same initial conditions, randomly chosen between 0 and  $u_{th}$ .

For small values of  $R < 20$  ( $d < 0.08$ ) and  $\sigma \leq 0.4$ , complete  $\omega$ -synchronization settles in the system (see Fig. 8a), as in the case of simple diagonal coupling. By gradually increasing the values of the coupling range, we first observe a chimera-like state, meaning the simultaneous existence of a dominant synchronization and a few asynchronous “rebels”, see Fig. 8b. As we will see in the

next section, sec. IV B, keeping  $R = \text{const.}$  and gradually increasing the  $\sigma$  values, these rebels turn into bigger incoherent clusters, giving rise to typical chimera states. Rebels, also known as solitary states have been previously reported in [55] for the Kuramoto model with inertia and for small values of the coupling range (see also [53, 54, 56]). In the LIF model, as  $R$  increases beyond  $R = 150$  ( $d = 0.6$ ), the solitaires grow in numbers forming aggregates, and ultimately turn into the incoherent domains of the classical chimeras. Comparing Figs. 8b and c, we observe how the mean phase velocity profile of the incoherent regions broadens as  $R$  increases. For even larger values of the coupling range, e.g.  $R = 200$ , chimera states become more prominent or the system returns to a state of complete synchronization.

The spatiotemporal evolution of the system for a small value of the coupling strength  $\sigma = 0.4$  and for a variation of the coupling radius  $R$  in the nonlocal and in the diagonal neighborhoods, are demonstrated in Fig. 8. As previously, for small values of  $R$  we observe complete synchronization while for intermediate  $R$  values a few desynchronized solitaires appear. These solitaires are organized in four different groups and can be spotted in the spacetime plots (right panels) and the mean phase velocity plots (middle panels). The spacetime plots are depicted for a small time window for image resolution purposes. Looking closer to the mean phase velocity profiles we distinguish that in the region where the solitaires appear the  $\omega$ 's take values in the range  $\omega \in (1.8 - 1.9)$ .

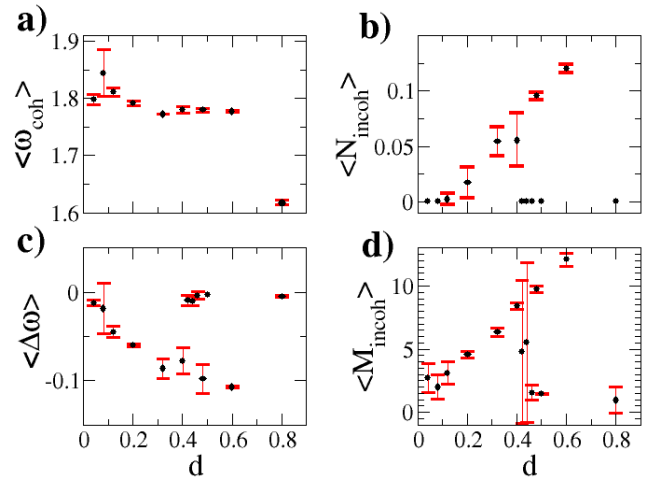


FIG. 9: (Color online) Measures of coherence and incoherence for different values of the coupling ratio  $d$ .  $\sigma = 0.4$  and all other parameters are as in Fig. 8.

Figure 9 displays measures of coherence and incoherence as a function of the coupling range, for small  $\sigma$  values ( $\sigma = 0.4$ ). Each point represents an average over fourteen different initial conditions. Figure 9c demonstrates that synchronization settles in the system for very small and

for very large values of the coupling range  $R$ . The synchronization at large coupling ranges is not surprising, since the system reaches an all-to-all connectivity in this limit. In the region of small  $R$  the mean phase velocity of the coherent regions is found approximately constant (around  $\omega \sim 1.8$ ), while it drops as we approach the all-to-all connectivity (see Fig. 9a). As  $(4R + 1) \rightarrow N$  the system slows down while synchronizing and this is expressed by a smaller value of the mean phase velocity (e.g. for  $d = 0.801$  where  $\omega \sim 1.6$ ). Figure 9b shows that the population of the incoherent elements increases as the coupling ratio  $d$  increases, up to  $d = 0.801$  when it drops back to zero, which reflects the complete synchronization in the large  $d$  limit. The difference of the  $\omega$ 's of the coherent and incoherent elements,  $\Delta\omega$ , increases gradually as the coupling ratio  $d$  increases. Since the  $\langle \omega_{\text{coh}} \rangle$  remains approximately constant with the increase of  $d$ , we conclude that the incoherent domains become more active. As expected,  $\Delta\omega$  is zero for complete synchronization (i.e.  $d = 0.041$ ,  $d = 0.801$ ). This is also reflected by the evolution of  $\langle N_{\text{incoh}} \rangle$  and  $\langle M_{\text{incoh}} \rangle$ . Both  $\langle N_{\text{incoh}} \rangle$  and  $\langle M_{\text{incoh}} \rangle$  receive their maximum values when  $\Delta\omega$  is also maximum, thus suggesting that the incoherent domains become more pronounced. Overall, the  $\langle N_{\text{incoh}} \rangle$  and  $\langle M_{\text{incoh}} \rangle$  absolute values are low indicating that the small  $\sigma$  values form “weak-chimeras”, consisting mainly of synchronous regions interrupted by few “rebels”.

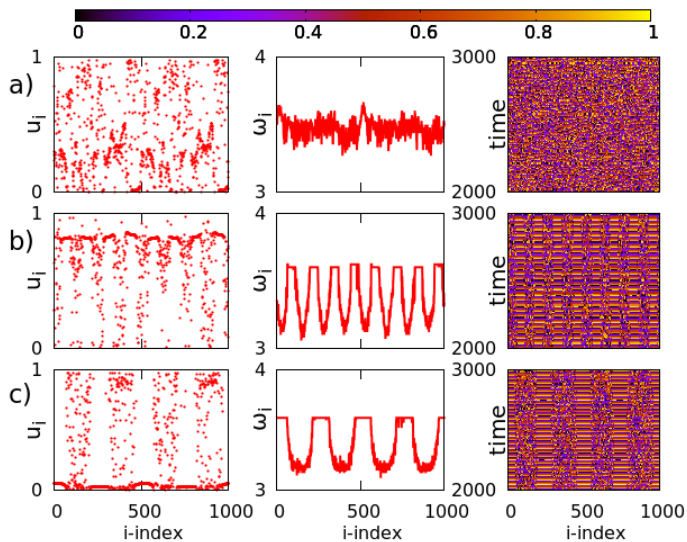


FIG. 10: (Color online) LIF system with superposition of nonlocal and diagonal connectivity: Typical snapshots (left column), mean-phase velocity (middle column) and space-time plots (right column). a)  $R = 10$  ( $d=0.041$ ), b)  $R = 100$  ( $d=0.401$ ) and c)  $R = 150$  ( $d=0.601$ ). Other parameters are  $\sigma = 1.6$ ,  $N = 1000$ ,  $\mu = 1$  and  $u_{\text{th}} = 0.98$ . All realizations start from the same initial conditions, randomly chosen between 0 and  $u_{\text{th}}$ .

Let us now discuss the spatiotemporal evolution of the system for a greater value of the coupling strength,

$\sigma = 1.6$ , demonstrated in Fig. 10. Again for very small values of the coupling range  $R$  the system does not support chimera states, see Fig. 10a. As in the case of Fig. 8a, when the coupling strength is weak and the coupling range is very small the coupled elements do not significantly alter the local dynamics; instead, they all keep common  $\omega$ 's very close to the uncoupled system while their phases remain asynchronous. As the coupling strength increases the coupled elements have a stronger bond and the system is driven into forming chimeras. Furthermore, we note that as the coupling range increases the multiplicity of the chimera states decreases. For example, for  $R = 100$  we observe an eight-headed chimera (Fig. 10b) and for  $R = 150$  we observe a four-headed chimera (Fig. 10c).

Returning to the map, Fig. 7, different  $(d - \sigma)$  pairs result in different multi-headed chimeras. We note that some pairs serve as borderlines between the different multi-head chimera areas or pure synchronous and asynchronous regimes. The steady state of these “borderline” pairs may be affected by the states of surrounding regions and usually result into one or another multi-headed chimera, depending on the initial conditions. An example of this behavior is reported in the case of Fig. 10c, in which according to Fig. 7 the system sets to either a six-headed or a four-headed chimera (shown in this figure).

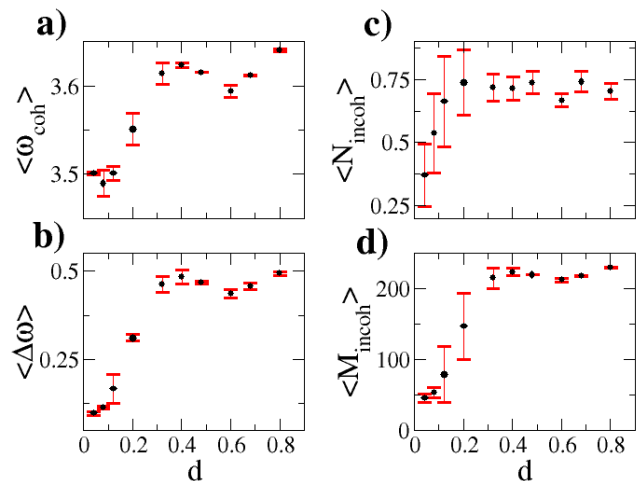


FIG. 11: (Color online) Measures of coherence and incoherence for different values of the coupling ratio  $d$ .  $\sigma = 1.6$  and all other parameters are as in Fig. 8. Averages are taken over 14 initial conditions.

The measures of coherence and incoherence in this case are demonstrated in Fig. 11. Overall, we note that the values of the coherent mean phase velocities are higher compared to the ones in Fig. 9. This along with the plots in Fig. 10, shows that for higher values of the coupling strength the coherent regimes have higher values of the mean phase velocity. When  $\langle \omega_{\text{coh}} \rangle$  receives its maximum



and minimum value the same happens accordingly for the  $\Delta\omega$ .  $\langle N_{\text{incoh}} \rangle$  and  $\langle M_{\text{incoh}} \rangle$  receive higher values than in Fig. 9. This is expected as the incoherent clusters are bigger in size and chimera states are formed. Furthermore,  $\langle N_{\text{incoh}} \rangle$  and  $\langle M_{\text{incoh}} \rangle$  increase as the coupling ratio  $d$  increases up to  $d = 0.401$  and thenceforth remain approximately constant. This means that the incoherent population does not significantly change after a certain point.

Comparing Figs. 9 and 11, it becomes evident that for smaller values of the coupling strength (Fig. 9) the incoherent domains increase in population for the larger values of the coupling radius. Interestingly, this is not the case for greater values of  $\sigma$  such as shown in Fig. 11. In the latter, the incoherent domains gradually increase in population as the coupling ratio  $d$  increases until  $d \geq 0.2$  after which point the population remains approximately constant. These observations come to agreement with the imprint of the chimera states on the map in Fig. 7.

Overall, the measures of coherence indicate that as the coupling range increases (below all-to-all coupling) the emergence of chimera states is favored and the mean phase velocity deviations between coherent and incoherent regions become more prominent. This holds for all values of  $\sigma$  outside the transition region.

### B. Combined connectivity with variation of the coupling strength

In this subsection we systematically vary the coupling strength and discuss the effect of this tuning on the synchronization patterns and on the chimera morphology. As before, the neurons are set on a regular ring topology and with the same connectivity scheme, initial conditions and parameters as in subsection IV A.

We scan the system over different values of the coupling strength  $\sigma$  and for coupling range  $R = 120$  and present the spatiotemporal evolution in Fig. 12. We first note that the mean phase velocity  $\omega$  overall increases with  $\sigma$  and the solitaires developed from small  $\sigma$  (Fig. 12a) grow gradually to form typical chimeras (Fig. 12b). We observe that for small values of the coupling strength the coherent regimes have higher  $\omega$  values than the incoherent regimes (see Fig. 12a,b, middle panels). Surprisingly, this behavior is inverted when  $\sigma$  takes values greater than 1. In this case the elements belonging to the incoherent regimes have higher  $\omega$ 's than in the coherent regimes (compare middle panels in Figs. 12a,b and 12d).

For values of the coupling strength in the range  $1.0 \leq \sigma < 1.5$  (with  $R < 200$ ,  $d < 0.801$ ) complete  $\omega$ -synchronization is observed, where all elements acquire common mean phase velocity, but their phases might be asynchronous. The precise size of the  $\sigma$ -range where complete  $\omega$ -synchronization is observed depends on the value of  $R$ . E.g., for  $R = 200$  complete  $\omega$ -synchronization is observed for  $1 \leq \sigma \leq 1.5$ , while for other values of  $R$  the range of  $\sigma$  which supports complete  $\omega$ -

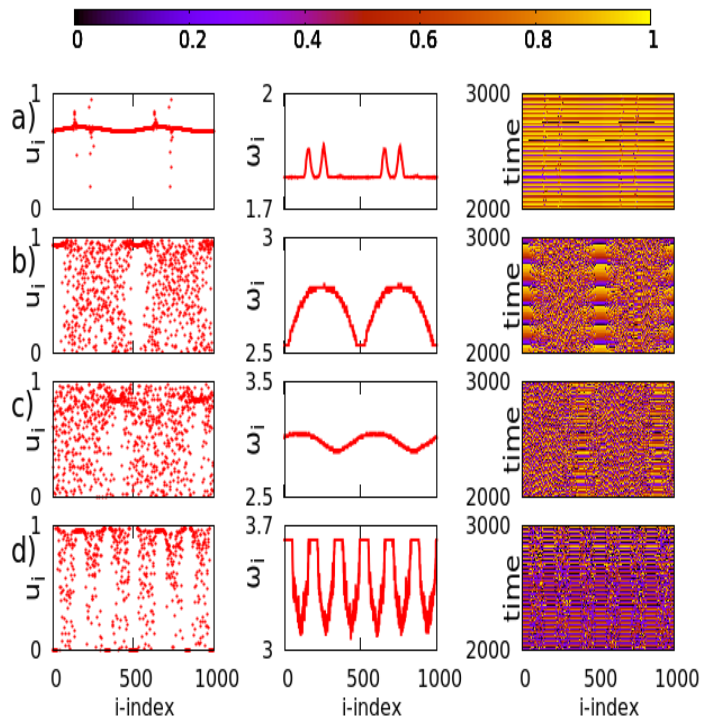


FIG. 12: (Color online) LIF system with superposition of nonlocal and diagonal connectivity: Typical snapshots (left column), mean-phase velocity (middle column) and space-time plots (right column). a)  $\sigma = 0.4$ , b)  $\sigma = 0.6$ , c)  $\sigma = 0.8$  and d)  $\sigma = 1.6$ . Other parameters are  $R = 120$  ( $d = 0.481$ ),  $N = 1000$ ,  $\mu = 1$  and  $u_{\text{th}} = 0.98$ . All realizations start from the same initial conditions, randomly chosen between 0 and  $u_{\text{th}}$ .

synchronization might be different.

Looking further to the measures of coherence and incoherence as a function of the coupling strength, Fig. 13, for both  $d = 0.481, 0.801$  we notice the increase of  $\langle w_{\text{coh}} \rangle$  as the coupling strength becomes stronger. For  $\sigma = 1.0$ ,  $\sigma = 1.2$  and  $\sigma = 1.4$  the  $\omega$ -values do not change drastically for finite system sizes. In these cases, complete  $\omega$ -synchronization is observed followed by phase desynchronization. Despite all elements being completely desynchronized (they all have different phases) they do not have significantly distinguishable  $\omega$ 's. Therefore, the state of complete phase desynchronization around  $\sigma = 1$  is characterized by coherence in respect to the distribution of the  $\omega$ 's.

$\langle \Delta\omega \rangle$  and  $\langle M_{\text{incoh}} \rangle$  are also increasing as  $\sigma$  increases and receive their highest values at the same point as  $\langle \omega_{\text{coh}} \rangle$ .  $\langle \Delta\omega \rangle$  and  $\langle M_{\text{incoh}} \rangle$  are equal or almost equal to zero for values of the coupling strength  $\sigma = 1.0, \sigma = 1.2$  and  $\sigma = 1.4$ , as a result of the approximately constant values of the  $\omega$ 's in these cases. The number of the incoherent elements,  $\langle N_{\text{incoh}} \rangle$ , increases with the increase of  $\sigma$  up to  $\sigma = 0.6$  and does not significantly change thereafter. For  $\sigma = 1.0, \sigma = 1.2$  and  $\sigma = 1.4$  all elements are  $\omega$ -synchronous, therefore

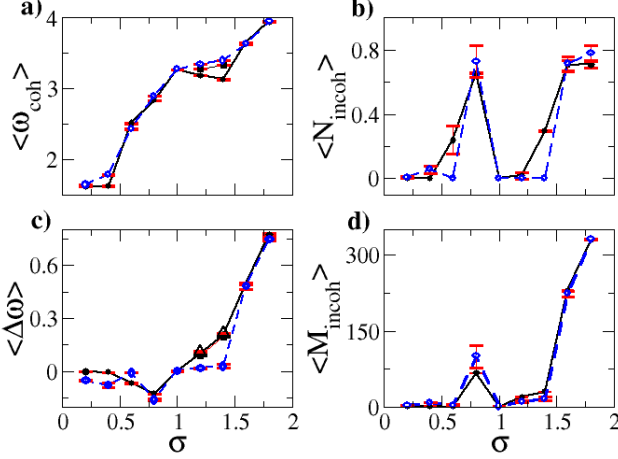


FIG. 13: (Color online) Measures of coherence and incoherence for different values of the coupling strength  $\sigma$  and for  $R = 120$ ,  $d = 0.481$  (blue-dashed lines) and  $R = 200$ ,  $d = 0.801$  (black-solid lines). All other parameters are as in Fig. 8. Averages are taken over 14 initial conditions.

$\langle N_{\text{incoh}} \rangle = \langle M_{\text{incoh}} \rangle = 0$  for these areas, even though they are phase asynchronous.

For larger values of the coupling range, e.g.  $R \geq 200$ , and within the same  $\sigma$ -range ( $1.0 \leq \sigma < 1.5$ ) we note that the synchronized regimes are divided into two subgroups with different frequencies. These two subgroups are shown in Fig. 13a,c, where the two coherent domains are depicted with a black circle and a black triangle for  $\sigma = 1.2$  and  $\sigma = 1.4$ , respectively. This effect will be discussed in detail in sec. IV C. Another observation is that in the case of ( $\sigma = 1.8, R = 200$ ) a four-headed chimera appears along with two smaller incoherent regions. Interestingly this four-headed chimera consists of wider incoherent/coherent regimes and of additional smaller incoherent regions similar to solitary states. This is further discussed in Appendix A.

Overall,  $\omega$ -inversion between coherent and incoherent regions takes place when  $\sigma$  crosses the value 1. Around  $\sigma = 1$  complete  $\omega$ -synchronization takes place, while the precise  $\sigma$ -range where complete  $\omega$ -synchronization is observed depends on the value of  $R$ . For even larger values of  $\sigma$  the phenomenon of two-level synchronization is observed which also depends both on  $\sigma$  and  $R$ , and will be further discussed in the next section.

### C. Two-level synchronization chimeras

In this subsection we discuss in more detail the two-level synchronization which has been recorded for relatively large values of  $\sigma$  and  $R$ . As working parameters we will use  $\sigma = 1.2 - 1.5$  and  $R = 200$ ,  $N = 1000$ ,

$\mu = 1$  and  $u_{\text{th}} = 0.98$ . As demonstrated in the previous sections for values of the coupling strength  $\sigma < 1$  the coherent domains of the chimera states have lower mean phase velocity values compared to the incoherent ones, whereas for  $\sigma \geq 1.6$  the opposite is observed. Therefore, certain areas such as  $[\sigma = 1.2, d = 0.801]$  and  $[\sigma = 1.4, d = 0.801]$  behave like border areas and the system presents two-level synchronization.

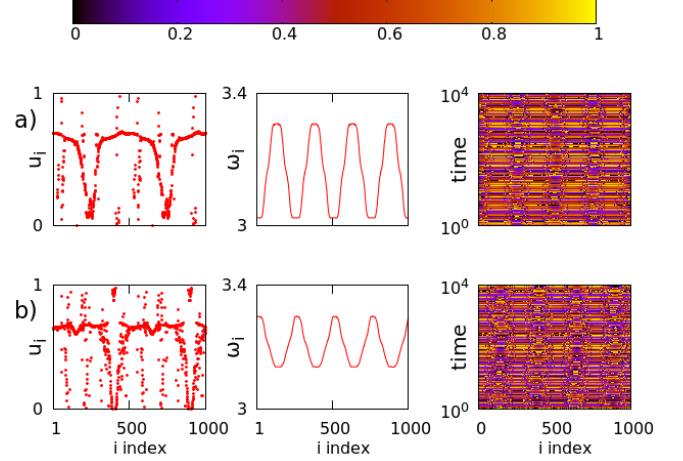


FIG. 14: (Color online) LIF system with superposition of nonlocal and diagonal connectivity: Mean-phase velocities (left column) and spacetime plots (right column). a)  $\sigma = 1.2$ , b)  $\sigma = 1.4$ . Other parameters are  $R = 200$  ( $d = 0.801$ ),  $N = 1000$ ,  $\mu = 1$  and  $u_{\text{th}} = 0.98$ . All realizations start from the same initial conditions, randomly chosen between 0 and  $u_{\text{th}}$ .

Figure 14 presents the mean phase velocities and spacetime plots for the previously mentioned parameters. Looking at the spacetime plots in Fig. 14a (right panel) one simply observes the formation of 8 incoherent regions mediated by 8 coherent regions. This is nothing exceptional, however, by looking at the mean phase velocity profiles, one observes that the 8 coherent regions are split in two groups: one group is characterized by high mean phase velocity,  $\omega_{\text{coh1}}$  while the other one is characterized with low mean phase velocity,  $\omega_{\text{coh2}}$ . The members of the two groups alternate, while the incoherent elements have  $\omega$ 's that lay on the sloping line between the two groups. The same observations hold for different values of  $\sigma$  as shown in Fig. 14b, but the difference between the two coherent levels vary with the coupling constant.

For this two-level synchronization it is not possible to use the classical rules described in refs. [24] to calculate the measures of coherence and incoherence. We now introduce a new algorithmic scheme which allows us to distinguish between the two regimes of coherence:

- First we calculate the maximum  $\langle \omega_{\text{coh1}} \rangle$  and the minimum  $\langle \omega_{\text{coh2}} \rangle$  values of the mean phase velocities. These two values characterize the mean frequency in each of the two synchronization levels.

- For the calculations of the  $N_{\text{incoh}}$  we set a small tolerance (e.g.,  $a = 0.01$ ), that serves as a border between the coherent and incoherent domains.
- We set the counter  $N_{\text{incoh}} = 0$  and we scan all elements,  $i = 1, \dots, N$ , to calculate the difference of the mean phase velocities between element  $i$  and each one of the coherent domains  $\langle \omega_{\text{coh1}} \rangle - \omega_i$  and  $\omega_i - \langle \omega_{\text{coh2}} \rangle$ . If  $[\langle \omega_{\text{coh1}} \rangle - \omega_i] > a$  and  $[\omega_i - \langle \omega_{\text{coh2}} \rangle] > a$  then we consider element  $i$  as belonging to the incoherent domain and we increase the counter  $N_{\text{incoh}} = N_{\text{incoh}} + 1$ .
- When all elements are scanned we normalize the counter  $N_{\text{incoh}} \rightarrow N_{\text{incoh}}/N$ .

Results of the two synchronization levels  $\langle \omega_{\text{coh1}} \rangle$ ,  $\langle \omega_{\text{coh2}} \rangle$ ,  $\Delta\omega_{\text{coh}} = \langle \omega_{\text{coh1}} \rangle - \langle \omega_{\text{coh2}} \rangle$  and  $\langle N_{\text{incoh}} \rangle$  are demonstrated in Fig. 15 (top). We note that the synchronization highest level,  $\langle \omega_{\text{coh1}} \rangle$ , does not significantly increase with the coupling strength  $\sigma$  for values  $1.2 < \sigma < 1.55$  while it decreases thereafter, see Fig. 15a. On the contrary, the lowest synchronization level,  $\langle \omega_{\text{coh2}} \rangle$ , decreases as  $\sigma$  increases. In this interval,  $1.2 < \sigma < 1.55$ , the difference between the  $\omega$ 's of the two synchronization levels increases with  $\sigma$ , as seen in Fig. 15 (middle row) and by comparison between Figs. 14a and b. The measure  $\langle N_{\text{incoh}} \rangle$  does not show a significant change in this parameter area. For values of  $\sigma > 1.55$  the two synchronization levels tend to approach one another. The latter along with the previous observations on the increase of  $\langle \omega_{\text{coh2}} \rangle$ , suggests that the elements following this synchronization scenario merge with the incoherent domains as  $\sigma$  increases. This gradually leads to the chimera states that appear for higher values of  $\sigma$ , i.e.  $\sigma = 1.6$ , where the coherent domains have higher  $\omega$  values and only one synchronization level is observed.

Based on the appearance of two sets of coherent regions with different mean phase velocities we propose here a possible scenario for the creation of chimera states. It is possible that due to the influence of the neighbors and for some parameter regions the coupled elements acquire bistable equilibrium states, i.e., they can be found in two frequency regimes, called  $\omega_{\text{coh1}}$  and  $\omega_{\text{coh2}}$ . Under the dynamics and due to the initial conditions some of them tend to the equilibrium frequency  $\omega_{\text{coh1}}$  forming domains around them, while others tend to the second equilibrium  $\omega_{\text{coh2}}$ . The elements in-between are influenced by both domains and acquire progressive frequency values, bridging the gap. Therefore, they behave incoherently because they have different frequencies. This scenario of bistable coupled elements can be used as a generic scenario for the formation of chimera states. Even in the case where only one synchronization level is evident while the incoherent regions are viewed as arc-shaped in the mean phase velocity profiles, one may imagine the presence of a second, non-visible (not well formed) level of synchronization at the top of the arc. This scenario may be supported by

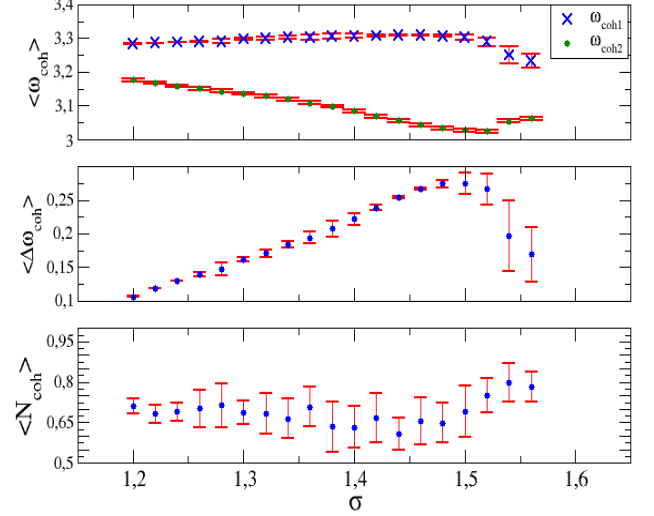


FIG. 15: (Color online) Measures of coherence for LIF system with superposition of nonlocal and diagonal connectivity for two-level synchronization. Parameter values are:  $R = 200$  ( $d = 0.801$ ),  $N = 1000$ ,  $\mu = 1$  and  $u_{\text{th}} = 0.98$ . All realizations start from initial potentials randomly chosen between 0 and  $u_{\text{th}}$  and averages are taken over 14 initial conditions.

findings in ref. [43] where even three levels of synchronization are realized, see sec. 4 and figures therein.

## V. CONCLUSIONS

In the current study we discuss the influence of a) diagonal connectivity and b) the combination of nonlocal-diagonal connectivity in the dynamics and especially in the appearance of chimera states in a network of LIF elements. We demonstrate that different connectivities influence the dynamics of the system and especially the presence and form of chimera states.

We show that the multiplicity of the chimera states is modulated by the values of the coupling range and the coupling strength and we identify areas in the  $(d, \sigma)$  parameter space where the system develops different behaviors. We show numerically that the mean phase velocity is not significantly affected by the variation of the coupling radius; instead, the variation of the coupling strength tunes the  $\omega$  values. More specifically, the  $\omega$ 's increase overall as the coupling strength increases. This is intuitively expected since a high value of the coupling strength amplifies the intensity of the interaction between different elements, which synchronize by dragging each other.

We stress the development of two new chimera patterns which emerge for relatively large values of the coupling

constant:

1. The two-level chimera states: these are states which consist of two groups of coherent states, one with low mean phase velocity and one with high. The elements of the two groups alternate, while the incoherent regions ensure the continuity of the  $\omega$ -profiles and serve to bridge the gap between the regions of low and high mean phase velocities.
2. The instability which develops in the middle of the coherent regions giving rise to “rebels” or solitary states. These solitary states build up to become incoherent regions as the coupling constant  $\sigma$  decreases.

Based on the 1st case (bi-leveled coherent domains), we propose a generic scenario on the formation of chimera states based on bistable element interactions.

In previous studies the influence of the refractory period in the nonlocal and reflecting connectivity cases was studied and it was shown that it affects drastically the chimera multiplicity and synchronization patterns in general. Since the refractory period is observed in biological neurons, it would be interesting to investigate its effects in the network with diagonal and combined connectivity. Another open question worth investigating is whether the novel effects (two-level synchronization, inversion of coherence, solitary to chimera growth) caused by the combined, nonlocal-diagonal connectivity in the LIF model are generic in many neuron models, or they are restricted to the LIF model which is characterized by the abrupt resettings of the potential. Combined connectivity effects are worth studying in the FitzHugh-Nagumo oscillator, the Hindmarsh-Rose model and Stuart-Landau oscillator and other models assimilating the activity of neurons. Problems related to memory effects in chains of nonlinear oscillators are also relevant for further studies, in the sense that the final states depend highly on the initial conditions (potentials) of the oscillators. This is a hard problem (see [59] and references therein) when a large number of oscillators are considered and is more tractable in small networks composed by a few oscillators.

### Acknowledgements

The authors would like to thank Prof. N. Sarlis and Dr. J. Hizanidis for helpful discussions. This work was supported by computational time granted from the Greek Research & Technology Network (GRNET) in the National HPC facility - ARIS - under project ID PA002002. NTD acknowledges financial support from the IKY Greek State Scholarship Foundation.

### Author Contribution Statements

NTD, IK and GK performed the numerical studies. NTD and AP participated to the designing of the study and to the coordination of the project. All authors con-

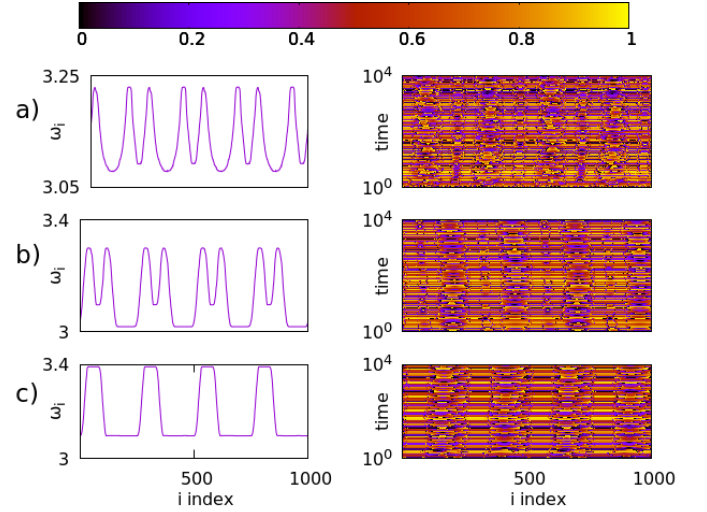


FIG. 16: (Color online) LIF system with superposition of nonlocal and diagonal connectivity: mean-phase velocity (left) and space-time plots (right). Parameters are: a)  $\sigma = 1.3$ ,  $R = 230$ , ( $d = 0.921$ ); b)  $\sigma = 1.6$ ,  $R = 230$ , ( $d = 0.921$ ); and c)  $\sigma = 1.7$ ,  $R = 230$ , ( $d = 0.921$ ). Other parameters are  $N = 1000$ ,  $\mu = 1$ , and  $u_{th} = 0.98$ .

tributed to the draft of the manuscript. All authors read and approved the final manuscript.

### Appendix A: Instabilities due to large values of the coupling constant

The dynamics of the LIF model allows for increasing the coupling strength arbitrarily high. Due to the condition 1b the potentials  $u_i$  never diverge as they are always reset to zero when they increase above the threshold  $u_{th}$ . This is a particularity of the LIF system, while most oscillators become unstable when the coupling strength  $\sigma$  increases beyond a critical value. Therefore, we have the opportunity to explore the network dynamics under very large values of the coupling strength. An example of the complexity induced is an instability within the synchronous regions which leads to the formation of asynchronous regions of smaller width than the synchronous ones. This instability is visible for large  $\sigma$  values as was also discussed in sec. IV C. The formation of the instability is visible in Fig. 16. Here the coupling strength values are  $\sigma = 1.3 - 1.8$ , while all other parameters are as in Fig. 14. The spacetime plots clearly indicate the formation of two large and two smaller incoherent regions separated by coherent regions.

By looking at the spacetime plots, as  $\sigma$  decreases from 1.7 (Fig. 16c) to 1.6 (Fig. 16b) one instability is created in the middle of the synchronous regions and four secondary, smaller synchronous regions appear. The size of the secondary regions increases as  $\sigma$  decreases from 1.6 (Fig. 16b) to 1.3 (Fig. 16a) and for even smaller  $\sigma$  eight coherent regions of equal sizes appear (not shown). The



same effect can be also seen in Figs. 3 and 5 for different parameter values where one new asynchronous region is created in the middle of the single synchronous domain.

By looking at the  $\omega$  profiles in Figs. 16 we note that the instabilities set in the synchronous regions having the largest mean phase velocity  $\omega_{\text{coh1}}$ , while the coherent regions with low mean phase velocity  $\omega_{\text{coh2}}$  are not affected.

The  $\omega$ 's in the new incoherent regions decrease gradually with  $\sigma$  and they approach  $\omega_{\text{coh2}}$  when eight coherent regions of equal sizes are formed, around  $\sigma = 1.2$  (not shown). The mechanism causing this second instability in large values of the coupling constant is not completely understood.

- 
- [1] E. S. Finn et al., Functional connectome fingerprinting: identifying individuals using patterns of brain connectivity, *Nature Neuroscience*, **18**, 1664–1671 (2016).
  - [2] N. K. Logothetis, What we can do and what we cannot do with fMRI (Review), *Nature*, **453**, 869–878 (2008).
  - [3] R. A. Poldrack and M. J. Farah, Progress and challenges in probing the human brain, *Nature*, **526**, 371–379 (2015).
  - [4] C. Vasalou, E. D. Herzog, and M. A. Henson, Small-World Network Models of Intercellular Coupling Predict Enhanced Synchronization in the Suprachiasmatic Nucleus *Journal of Biological Rhythms*, **24**, 243–254 (2009).
  - [5] W. -K. Li, M. J. Hausknecht, P. Stone, M. D. Mauk, Using a million cell simulation of the cerebellum: Network scaling and task generality, *Neural Networks* **47**, 95–102 (2013).
  - [6] A. Alonso and R. R. Llinas, Subthreshold Na<sup>+</sup>-dependent theta-like rhythmicity in stellate cells of entorhinal cortex layer II, *Nature*, **342**, 175–177 (1989).
  - [7] S. R. Cobb, E. H. Buhl, K. Halasy, O. Paulsen and P. Somogyi, Synchronization of neuronal activity in hippocampus by individual GABAergic interneurons, *Nature*, **378**, 75–78 (1995).
  - [8] V. Vuksanović, P. Hövel, Functional connectivity of distant cortical regions: Role of remote synchronization and symmetry in interactions, *NeuroImage*, **97**, 1 (2014).
  - [9] V. Vuksanović, P. Hövel, Dynamic changes in network synchrony reveal resting-state functional networks, *Chaos*, **25**, 023116 (2015).
  - [10] P. Katsaloulis, D. A. Verganelakis, A. Provata, *Fractals* **17** 181-189 (2009).
  - [11] P. Expert, R. Lambiotte, D. Chialvo, K. Christensen, H. J. Jensen, D. J. Sharp, F. Turkheimer, Self-similar correlation function in brain resting-state functional magnetic resonance imaging, *Journal of the Royal Society Interface*, **8** 472-479 (2011).
  - [12] P. Katsaloulis, A. Ghosh, A. C. Philippe, A. Provata, R. Deriche, Fractality in the neuron axonal topography of the human brain based on 3-D diffusion MRI, *European Physical Journal B* **85**, 150 (2012).
  - [13] H. Haken, *Brain Dynamics, An Introduction to Models and Simulations*, Springer Series on Synergetics, Springer-Verlag, Berlin (2008).
  - [14] E. M. Izhikevich, *Dynamical systems in neuroscience: the geometry of excitability and bursting*, The MIT Press, Cambridge (2007).
  - [15] C. Wang, and J. Ma, A review and guidance for pattern selection in spatiotemporal system, *International Journal of Modern Physics B* **32**, 1830003 (2018).
  - [16] S. Guo, Y. Xu, C. Wang, W. Jin, A. Hobiny, and J. Ma, Collective response, synapse coupling and field coupling in neuronal network, *Chaos Solitons & Fractals*, **105**, 120-127 (2017).
  - [17] M. Lv, J. Ma, and Y. Yao, and F. Alzahrani, Synchronization and wave propagation in neuronal network under field coupling, *Sci. China Technol. Sci.*, p. 1-10, (2018). <https://doi.org/10.1007/s11431-018-9268-2>.
  - [18] M. J. Panaggio and D. Abrams, Chimera states: coexistence of coherence and incoherence in networks of coupled oscillators, *Nonlinearity*, **28**, R67 (2015).
  - [19] E. Schöll, Synchronization patterns and chimera states in complex networks: interplay of topology and dynamics, *European Physical Journal Special Topics*, **225**, 891919 (2016).
  - [20] S. Majhi, M. Perc, and D. Ghosh, Chimera states in uncoupled neurons induced by a multilayer structure, *Scientific Reports*, **6**, 39033 (2016).
  - [21] S. Majhi, M. Perc, and D. Ghosh, Chimera states in a multilayer network of coupled and uncoupled neurons *Chaos* **27**, 073109 (2017).
  - [22] J. Hizanidis, N. E. Kouvaris, G. Zamora-López, A. Díaz-Guilera and C. G. Antonopoulos, Chimera-like States in modular neural networks, *Scientific Reports*, **6**, 19845 (2016).
  - [23] Y. Zhu, Z. Zheng, and J. Yang, Chimera states on complex networks, *Physical Review E*, **89**, 022914 (2014).
  - [24] I. Omelchenko, A. Provata, J. Hizanidis, E. Schöll and P. Hövel, Robustness of chimera states for coupled FitzHugh-Nagumo oscillators, *Physical Review E*, **91**, 022917 (2015).
  - [25] Y. Kuramoto and D. Battogtokh, Coexistence of coherence and incoherence in nonlocally coupled phase oscillators, *Nonlinear Phenomena in Complex Systems*, **5**, 380 (2002).
  - [26] D. M. Abrams and S. H. Strogatz, Chimera states for coupled oscillators, *Physical Review Letters*, **93**, 174102 (2004).
  - [27] N. C. Rattenborg, C. J. Amlaner and S. L. Lima, Behavioral, neurophysiological and evolutionary perspectives on unihemispheric sleep, *Neuroscience and Biobehavioral Reviews*, **24**, 817 (2000).
  - [28] J. Hizanidis, V. Kanas, A. Bezerianos and T. Bountis, Chimera states in networks of nonlocally coupled Hindmarsh-Rose neuron models, *International Journal of Bifurcation and Chaos*, **24**, 03 (2014).
  - [29] B. K. Bera, D. Ghosh, and M. Lakshmanan, Chimera states in bursting neurons, *Physical Review E*, **93**, 012205 (2016).
  - [30] R. G. Andrzejak, C. Rummel, F. Mormann and K. Schindler, All together now: Analogies between chimera state collapses and epileptic seizures, *Scientific Reports*, **6**, 23000 (2016).
  - [31] Q. Dai, D. Liu, H. Cheng, H. Li and J. Yang, Two-frequency chimera state in a ring of nonlocally coupled



- Brusselators, PLoS ONE, **12**, e0187067 (2017).
- [32] Z.-M. Wu, H.-Y. Cheng, Y. Feng, H.-H. Li, Q.-L. Dai and J.-Z. Yang, Chimera states in bipartite networks of FitzHugh-Nagumo oscillators, *Frontiers of Physics*, **13**, 130503 (2018).
- [33] I. Omelchenko, O. E. Omel'chenko, P. Hövel and E. Schöll, When nonlocal coupling between oscillators becomes stronger: patched synchrony or multichimera states, *Physical Review Letters*, **110**, 224101 (2013).
- [34] A. Schmidt, T. Kasimatis, J. Hizanidis, A. Provata, and P. Hövel, Chimera patterns in two-dimensional networks of coupled neurons, *Physical Review E*, **95**, 032224 (2017).
- [35] E. M. Essaki Arumugam, and M. L. Spano, A chimeric path to neuronal synchronization, *Chaos*, **25**, 1.4905856 (2015).
- [36] B. K. Bera, and D. Ghosh, Chimera states in purely local delay-coupled oscillators, *Physical Review E*, **93**, 052223 (2016).
- [37] B. K. Bera, S. Majhi, D. Ghosh, and M. Perc, Chimera states: Effects of different coupling topologies, *Europhysics Letters*, **118**, 10001 (2017).
- [38] S. Kundu, S. Majhi, B. K. Bera, D. Ghosh, and M. Lakshmanan, Chimera states in two-dimensional networks of locally coupled oscillators, *Physical Review E*, **97**, 022201 (2018).
- [39] S. Majhi, and D. Ghosh, Alternating chimeras in networks of ephaptically coupled bursting neurons, *Chaos*, **28**, 083113 (2018).
- [40] S. Luciola and A. Politi, Irregular collective behavior of heterogeneous neural networks, *Physical Review E*, **105**, 158104 (2010).
- [41] S. Olmi, A. Politi and A. Torcini, Collective chaos in pulse-coupled neural networks, *Europhysics Letters*, **92**, 60007 (2010).
- [42] N. D. Tsigkri-DeSmedt, J. Hizanidis, P. Hövel and A. Provata, Multi-chimera states in the Leaky Integrate-and-Fire model, *Procedia Computer Science*, **66**, 13 (2015).
- [43] N. D. Tsigkri-DeSmedt, J. Hizanidis, E. Schöll, P. Hövel and A. Provata, Chimera states in the Leaky Integrate-and-Fire Model: Effects of Reflecting Connectivity, *European Physical Journal B*, **90:139**, (2017).
- [44] T. Kasimatis, J. Hizanidis and A. Provata, Three-dimensional chimera patterns in networks of spiking neuron oscillators, *Physical Review E*, **97**, 052213 (2018).
- [45] Y. Maistrenko, O. Sudakov, O. Osiv, and V. Maistrenko, Chimera states in three dimensions, *New Journal of Physics*, **17**, 073037 (2015).
- [46] V. Maistrenko, O. Sudakov, O. Osiv, Y. Maistrenko, Multiple scroll wave chimera states, *European Physical Journal: Special Topics*, **226**, 1867-1881 (2017).
- [47] N. D. Tsigkri-DeSmedt, J. Hizanidis, P. Hövel and A. Provata, Multi-Chimera States and Transitions in the Leaky Integrate-and-Fire Model with Nonlocal Coupling and Hierarchical Connectivity, *European Physical Journal Special Topics*, **225**, 11491164 (2016).
- [48] I. Omelchenko, Y. Maistrenko, P. Hövel and E. Schöll, Loss of coherence in dynamical networks: Spatial chaos and chimera states, *Physical Review Letters*, **106**, 234102 (2011).
- [49] N. Brunel and M. C. W. van Rossum, Lopicque's 1907 paper: from frogs to integrate-and-fire *Brain Research Bulletin*, **50**, 303304 (1999).
- [50] L. F. Abbott, Lopicques introduction of the integrate-and-fire model neuron (1907) *Biological Cybernetics*, **97**, 337 (2007).
- [51] I. Omelchenko, A. Zakharova, P. Hövel, J. Siebert and E. Schöll, Nonlinearity of nonlocal dynamics promotes multi-chimeras, *Chaos*, **25**, 083104 (2015).
- [52] J. Hizanidis, E. Panagakou, I. Omelchenko, E. Schöll, P. Hövel and A. Provata, *Physical Review E*, **92** 012915 (2015).
- [53] T. Kapitaniak, P. Kuzma, J. Wojewoda, K. Czołczynski and Y. Maistrenko, Imperfect chimera states for coupled pendula, *Scientific Reports*, **4**, 6379 (2014).
- [54] K. Premalatha, V. K. Chandrasekar, M. Senthilvelan and M. Lakshmanan, Imperfectly synchronized states and chimera states in two interacting populations of nonlocally coupled Stuart-Landau oscillators, *Physical Review E*, **94**, 012311 (2016).
- [55] P. Jaros, S. Brezetsky, R. Levchenko, D. Dudkowski, T. Kapitaniak, Y. Maistrenko, Solitary states for coupled oscillators with inertia, *Chaos*, **28**, 011103 (2018).
- [56] R. Gopal, V. K. Chandrasekar, D. V. Senthilkumar, A. Venkatesan and M. Lakshmanan, Chimera at the phase-flip transition of an ensemble of identical nonlinear oscillators, *Communications in Nonlinear Science and Numerical Simulation*, **59**, 30–46 (2018).
- [57] F. Mormann, K. Lehnertz, P. David, and C. E. Elger, Mean phase coherence as a measure for phase synchronization and its application to the EEG of epilepsy patients, *Physica D* **144**, 358 (2000).
- [58] F. Mormann, T. Kreuz, R. G. Andrzejak, P. David, K. Lehnertz, and C. E. Elger, Epileptic seizures are preceded by a decrease in synchronization, *Epilepsy Research* **53**, 173–185 (2003).
- [59] F.-Q. Wu, J. Ma, and G.-D. Ren, Synchronization stability between initial-dependent oscillators with periodical and chaotic oscillation, *Journal of Zhejiang University - Science A: Applied Physics & Engineering*. DOI: 10.1631/jzus.A1800334.